Medical Engineering and Physics 000 (2018) 1–9

Contents lists available at ScienceDirect

Medical Engineering and Physics

journal homepage: www.elsevier.com/locate/medengphy

# Shape-memory-alloy-based smart knee spacer for total knee arthroplasty: 3D CAD modelling and a computational study

Arvind Gautam[a], Miguel A Callejas[b], Amit Acharyya[a,*], Swati Ghosh Acharyya[c]

[a] Department of Electrical Engineering, Indian Institute of Technology, Hyderabad, India
[b] Department of Architecture, Seville, Spain
[c] School of Engineering Sciences & Technology, University of Hyderabad (UOH), Hyderabad, India

ARTICLE INFO

*Article history:*
Received 22 March 2017
Revised 10 March 2018
Accepted 13 March 2018
Available online xxx

*Keywords:*
SMA
PMMA
TKA
Knee osteoarthritis
CAD
Knee kinetics
Finite element analysis

ABSTRACT

This study introduced a shape memory alloy (SMA)-based smart knee spacer for total knee arthroplasty (TKA). Subsequently, a 3D CAD model of a smart tibial component of TKA was designed in Solidworks software, and verified using a finite element analysis in ANSYS Workbench. The two major properties of the SMA (NiTi), the pseudoelasticity (PE) and shape memory effect (SME), were exploited, modelled, and analysed for a TKA application. The effectiveness of the proposed model was verified in ANSYS Workbench through the finite element analysis (FEA) of the maximum deformation and equivalent (von Mises) stress distribution. The proposed model was also compared with a polymethylmethacrylate (PMMA)-based spacer for the upper portion of the tibial component for three subjects with body mass index (BMI) of 23.88, 31.09, and 38.39. The proposed SMA -based smart knee spacer contained 96.66978% less deformation with a standard deviation of 0.01738 than that of the corresponding PMMA based counterpart for the same load and flexion angle. Based on the maximum deformation analysis, the PMMA-based spacer had 30 times more permanent deformation than that of the proposed SMA-based spacer for the same load and flexion angle. The SME property of the lower portion of the tibial component for fixation of the spacer at its position was verified by an FEA in ANSYS. Wherein, a strain life-based fatigue analysis was performed and tested for the PE and SME built spacers through the FEA. Therefore, the SMA-based smart knee spacer eliminated the drawbacks of the PMMA-based spacer, including spacer fracture, loosening, dislocation, tilting or translation, and knee subluxation.



## 1. Introduction

Osteoarthritis is a common cause of disability pertaining to people aged 45–65 years, and athletes, as reported in [1–4]. Recent studies [5–9] showed that people with a body mass index (BMI) greater than 25 were prone to knee osteoarthritis. The main cause of knee osteoarthritis is the asymmetric loading of the medial and lateral compartment of the knee joint owing to a heavy body weight during different activities of daily life.

The knee joint is between two bones of the human body. The tibia and femur are comprised of two separate articulations: the tibiofemoral (TF) and patellofemoral (PF) joints. The six degrees of freedom of the motion of the knee are the three rotations, the flexion/extension, varus/valgus, and internal/external, and the three translations, the anterior/posterior, medial/lateral, and proximal/distal. Flexion and extension are the primary motions of the TF joint on the sagittal plane, which provide a maximum flexion of 160°, i.e., also referred to as the range of motion described in the study by Kuster et al. [13] and D'Lima et al. [14]. To extend the knee with minimal contraction of the quadriceps, the PF joint provides a three-dimensional range of motion across the TF joint flexion, as reported by Masouros et al. [12].

Polymethylmethacrylate (PMMA)-based total knee arthroplasty (TKA) is an effective method to treat knee osteoarthritis by placing a static or articulating PMMA cement antibiotic spacer between the femur and tibia, as reported in [15–21]. However, owing to asymmetric loading on the knee at different flexion angles after the treatment of an infected TKA by an articulating PMMA cement spacer for people above 45 years of age having osteoporosis, the survival of the PMMA artificial knee component is inadequate, according to the studies by Revell [22] and Struelens et al. [23]. The study by Struelens et al. [23] reported that 57% out of 154 patients faced spacer-related problems, such as spacer dislocation, fracture,

*Abbreviations:* BMI, body mass index; CAD, computer aided design; NiTi, nickel titanium; PE, pseudoelasticity; PF, patellofemoral; PMMA, polymethylmethacrylate; SMA, ahape memory alloy; SME, shape memory effect; TF, tibiofemoral; TKA, total knee arthroplasty; FEA, finite element analysis.

* Corresponding author.
*E-mail address:* amit_acharyya@iith.ac.in (A. Acharyya).

https://doi.org/10.1016/j.medengphy.2018.03.001
1350-4533/

loosening, tilting or translation, and knee subluxation. For the failure of PMMA-based TKA, an increased burden of the cost to the patient and health care system occurred, as described in the studies by Brunnekreef et al. [10] and Cui et al. [11]. Therefore, to solve the aforementioned problems, a 3D CAD model of the tibial component of TKA (smart knee spacer) based on the shape memory alloy (SMA) NiTi was proposed followed by a finite element analysis.

The SMA is a smart material with novel functionalities such as a high strength, high fatigue resistance, high resistance to wear, and biocompatibility. In addition, the SMA exhibits two unique properties: the shape memory effect (SME) and pseudoelasticity (PE), which provide an improvement over the existing state-of-the-art technologies for industrial as well as biomedical applications. In a biomedical application, Majid et al. [26] designed an SMA-based expandable pedicle screw to enhance fixation in osteoporotic bone. Petrini et al. [25] performed a computational study of the SMA behaviour for biomedical devices, and Bahraminasab et al. [31] showed the effect of the SMA on the stress distribution and contact pressure in a total knee replacement through an FEA.

This is the first study where both properties of the SMA were used to overcome the drawbacks of the state-of-the-art technology. The use of the SMA for TKA was proposed in the preliminary version of this study by Gautam et al. and was presented in Ref. [35]. In this study, the following was proposed.

1. The PE property-based upper portion of the tibial component was introduced from previously published research [35] by rigorous study through calculating the TF force of the knee joint for three subjects with BMIs of 23.88, 31.09, and 38.39 for different activities of daily life. A comparative study of the PE property-based tibial component with the PMMA-based technology was performed using an ANSYS-based finite element analysis for the maximum deformation and equivalent (von Mises) stress distribution.
2. Subsequently, the CAD model was proposed by exploiting the SME property of the SMA to improve the sustainability and long-term functionality of the tibial component for loosening of the spacer at different unsymmetrical loadings for the osteoporotic bone.
3. Finally, the efficacy of the PE and SME properties of the NiTi built proposed smart tibial component of TKA was verified by a strain life-based fatigue analysis using the FEA in ANSYS Workbench.

## 2. Motivation and background

### 2.1. Shape memory mechanism

The SMA, as mentioned in the previous section, exhibits unique properties of the SME and PE [36]. Therefore, SMA can regain its original shape or size after a large deformation beyond the elastic limit based on the applied loading, such as thermal loading for the SME and mechanical unloading for the PE, as shown in Figure 1(a) and described in the studies by Dai et al. [24], Jani et al. [27], Funakubo [28], Suzuki et al. [29], Buehler et al. [37], and Duerig and Pelton [39].

The SMA can be in two different solid phases by means of three different crystal structures, i.e., twinned martensite, detwinned martensite, and austenite, and five possible transformations among these crystal structures. The austenite and martensite phases are stable at high and low temperatures, respectively. Therefore, the phase transformation between martensite and austenite can be achieved by applying heat. This phase transformation from martensite to austenite starts at $A_s$ (the austenite start temperature) and ends at $A_f$ (the austenite finish temperature). During this phase transformation above temperature $T > A_s$, the material contracts and transforms to austenite by regaining its original shape. Upon cooling, the material transforms back to the martensite phase at $M_s$ (the martensite start temperature) and ends at $M_f$ (the martensite finish temperature). The highest temperature at which martensite can no longer be stress-induced is referred to as $M_d$, and above this temperature, the SMA can be permanently deformed like an ordinary material. The shape change phenomenon of the SMA, known as the SME and PE, are explained as follows.

1. SME: the SME maintains the deformed state after removal of the external force, and then returns to the original state by thermal loading at a certain temperature range.
2. PE: the SMA returns to the original shape when the load is released after a large deformation beyond the elastic limit at the constant temperature for range of $A_f < T < M_d$.

The SME and PE of the SMA are the diffusion-less solid phase transition between the martensite and austenite crystal structures. This behaviour of the SMA can be predicted from the crystallographic and thermodynamics of the material given in the literature by Petrini et al. [25], Funakubo et al. [28], and Suzuki et al. [29].

### 2.2. Load and constraints at the TF joint

Determining the force acting on the TF joint is critical. Numerous applicable assumptions are required owing to the complexity of the knee joint, as shown in the studies by Masouros et al. [12], Kuster et al. [13], and D'Lima et al. [14]. Based on the different activities performed by the lower limb, a delineative model of the human skeleton was designed for walking based on a person pressing the ground using a single foot, as shown in Figure 1(b). This situation is frequent and produces large load conditions at the knee. Thus, this situation was included in our study as a boundary condition for the computational analysis in ANSYS Workbench to show the robustness of the proposed model.

The SME and PE properties of the SMA NiTi were used for the design of the smart tibial component for the TKA components as follows.

1. The upper portion of the tibial component of TKA was made by using the PE property of the SMA. During different activities of daily life at a different flexion angles, the PE property of the SMA absorbed a large amount of stress and, if deformed, recovered its original shape upon unloading.
2. The lower portion of the tibial component was made using the SME property of the SMA. This would solve the problem of spacer loosening, dislocation, or translation under unsymmetrical loading at different flexion angles.

## 3. Proposed SMA-based TKA component

A 3D CAD design was proposed for the smart tibial component of TKA using the SMA NiTi, and the corresponding FEA was presented in ANSYS Workbench. Based on the experimental examinations for daily life activities available in the literature by Kuster et al. [13], Bahraminasab et al. [31], and Godest et al. [32], four configurations of flexion angles, i.e., 60°, 80°, 90°, and 115°, were studied for three subjects with BMIs of 23.88, 31.09, and 38.39. When a person used a single foot for performing daily life activities, the corresponding tibiofemoral bone-to-bone forces ($F_k$) were computed for all cases, as shown in Figure 2. These computed values of force were used as the input boundary conditions for the simulations of the tibial component of TKA in ANSYS Workbench. Assuming $F_k$' was the tibiofemoral force when a person used both feet for performing different daily life activities, $F_k$' was represented as shown below.

$$F'_k = 0.5F_k \quad (1)$$

Please cite this article as: A. Gautam et al., Shape-memory-alloy-based smart knee spacer for total knee arthroplasty: 3D CAD modelling and a computational study, Medical Engineering and Physics (2018), https://doi.org/10.1016/j.medengphy.2018.03.001

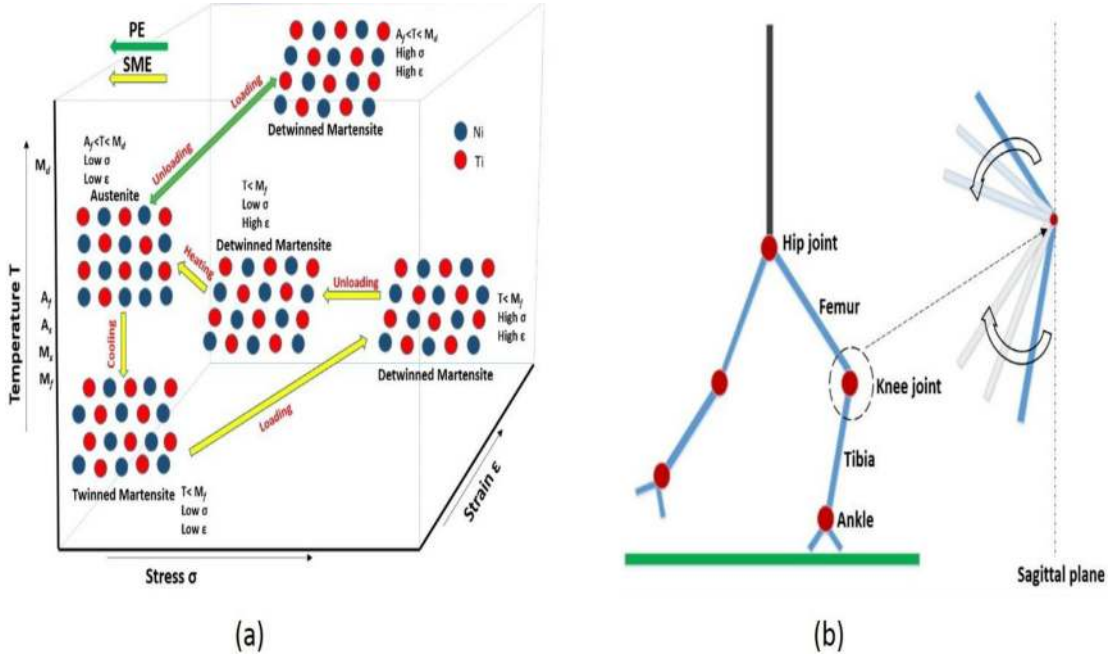


**Figure 1.** (a) Shape memory mechanism and (b) the model of the human skeleton while walking on the ground.

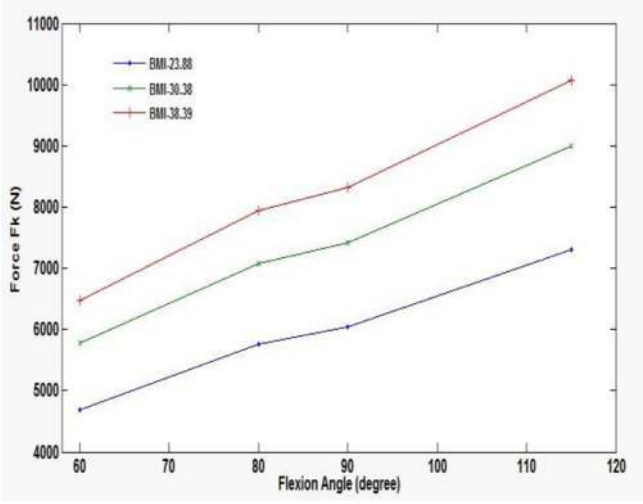


**Figure 2.** Tibiofemoral force comparison plot.

In this study, the tibiofemoral force ($F_k$') for level walking, climbing stairs, descending stairs, and sitting down were 2.99, 3.67, 3.84, and 4.66 times the body weight, respectively, were adopted from the studies by Kuster et al. [13], Collins [40], Morrison [41], Andriacchi et al. [42], Morrison [43], and Harrington [44].

### 3.1. Proposed CAD model and the FEA

TKA is a frequently performed surgical procedure in orthopaedic surgery. Patients suffering from knee osteoarthritis benefit from this operation through improvement in functionality and reduction in perceived pain [33]. TKA is an artificial joint usually made of a metallic alloy and plastic material that can replace the damaged knee completely or partially. The total prosthesis consists of two components: the femoral and tibial components tightly attached to the femur and tibia bone, respectively.

NiTi SMA was used, and the PE and SME properties were used to design a 3D CAD model of the state-of-the-art standard tibial component using CAD Solidworks software [34]. The step-wise flow is shown in Figure 3(a). Ingrassia et al. [30] designed two industrial standard total knee joint prostheses and compared their performance using an FEA. Godest et al. [32] performed an FEA for knee joint replacement during a gait cycle.

#### 3.1.1. PE property-based proposed CAD model for the upper portion of the tibial component

The proposed 3D CAD model of the tibial component was imported in the finite element commercial tool ANSYS Workbench and meshed with the hex dominant method of the solid elements, as shown in Figure 3(b). For the complete model, 21,142 of the total elements were used for the simulation [38]. Then, the tibial component was simulated by the SMA capability developed in the framework of ANSYS Workbench. The static structure application module was used to solve the problem wherein the PE property of the SMA NiTi was assigned to the upper portion of the designed CAD model with the material parameters listed in Table 1.

In the FEA of the tibial component, the lower face of the tibial component CAD model was fixed, and the tibiofemoral bone-to-bone force ($F_k$) was computed (as shown in Figure 2) for the three subjects, which were used as the input boundary conditions. The tibial component of the TKA spacer was tested for four flexion angles, i.e., 60°, 80°, 90°, and 115°, by the FEA on ANSYS Workbench. The simulations were carried out in two steps, where each step, to avoid simulation convergence, consisted of at least 200 sub-steps as explained below.

1. Step-I: in this step, a force at various flexion angles was applied on the top two faces of the tibial component whose property was assigned as the PE of the SMA for $T > A_f$, which transformed from austenite to the detwinned martensite phase with high-stress and high-strain values.
2. Step-II: in this step, the applied load (force) was released, and the tibial component relaxed, transformed from detwinned martensite to the austenite phase with low-stress and low-strain values.

Please cite this article as: A. Gautam et al., Shape-memory-alloy-based smart knee spacer for total knee arthroplasty: 3D CAD modelling and a computational study, Medical Engineering and Physics (2018), https://doi.org/10.1016/j.medengphy.2018.03.001

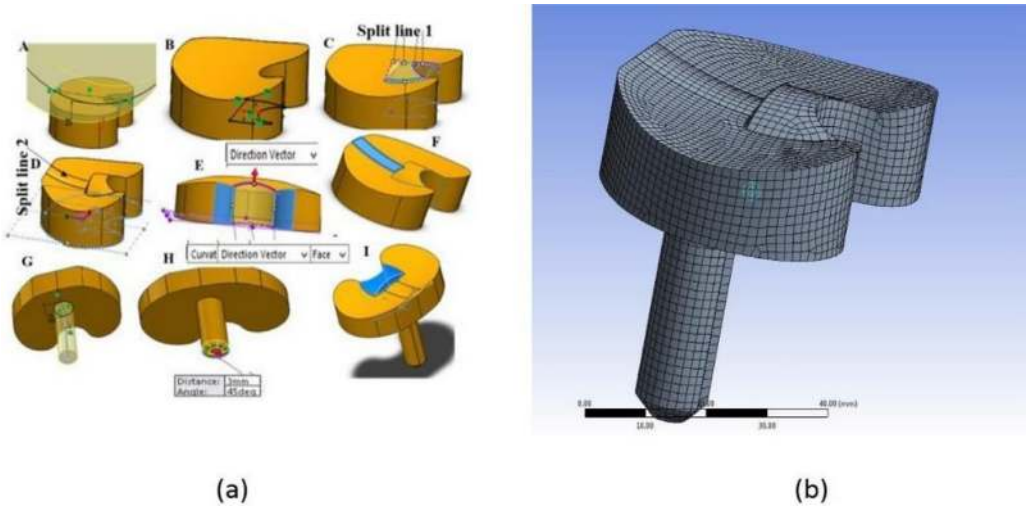


**Figure 3.** (a) Proposed CAD model. Image A shows the cutting of the extrude box. Image B shows split line 1, and image C shows the extruded upper surface of split line 1. Image D shows split line 2, and image E shows the boundary surface. Image F shows the extruded upper surface of split line 2, and image G shows the extruded lower surface a cylindrical rod. Image H shows a chamfer on the cylindrical rod at the lower end, and image I shows the complete CAD design. Picture (b) shows the meshed CAD model.

**Table 1**
Material properties of the NiTi SMA (PE).

| Parameter | Value |
|---|---|
| Sigma SAS | 520 MPa |
| Sigma FAS | 600 MPa |
| Sigma SSA | 300 MPa |
| Sigma FSA | 200 MPa |
| Epsilon | 0.07 $mm^{-1}$ |
| Alpha | .01 |
| Young's modulus | 60,000 MPa |
| Poisson's ratio | .33 |

**Table 2**
Material properties of the NiTi SMA (SME).

| Parameter | Value |
|---|---|
| Hardening parameter | 500 MPa |
| Reference temperature | 23 °C |
| Elastic limit | 120 MPa |
| Temp. scaling parameter | 8.3 |
| Max. transformation strain | 0.07 $mm^{-1}$ |
| Martensite modulus | 70,000 MPa |
| Load dependency parameter | 0 |
| Young's modulus | 60,000 MPa |
| Poisson's ratio | .33 |

*3.1.2. SME property-based CAD model for the lower portion of the tibial component*

To improve the sustainability and long-term functionality of the TKA component (tibial component) at different asymmetrical loadings, the lower portion of the tibial component was designed using the SME property of NiTi. To study the SME effect in the FEA, the 3D CAD model was designed. This model consisted of two parts: the tibial component with a hollow lower portion and four cylindrical tools positioned opposite each other, as shown in Figure 4(a). The complete 3D CAD model was then meshed with the adaptive size function with coarse meshing, as shown in Figure 4(b). The total number of elements and nodes used for this complete model was 856 and 5083, respectively. The static structural application module was used to solve the problem by assigning the SME material parameter to the lower hollow portion of the tibial component, as listed in Table 2.

In the FEA-based study, for the SME property of the tibial component, four cylindrical tools were used to compress the lower portion of the tibial component by 2 mm before inserting the component into the tibia at room temperature (22 °C). After deformation, the spacer was assumed to be inserted into the tibia bone (at the

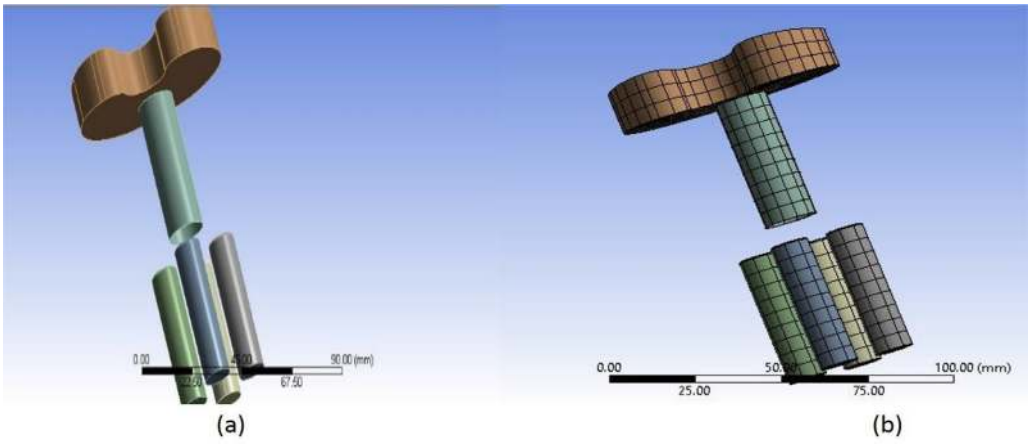


**Figure 4.** (a) Proposed CAD model for the SME property and (b) the meshed CAD model for the SME property.

Please cite this article as: A. Gautam et al., Shape-memory-alloy-based smart knee spacer for total knee arthroplasty: 3D CAD modelling and a computational study, Medical Engineering and Physics (2018), https://doi.org/10.1016/j.medengphy.2018.03.001

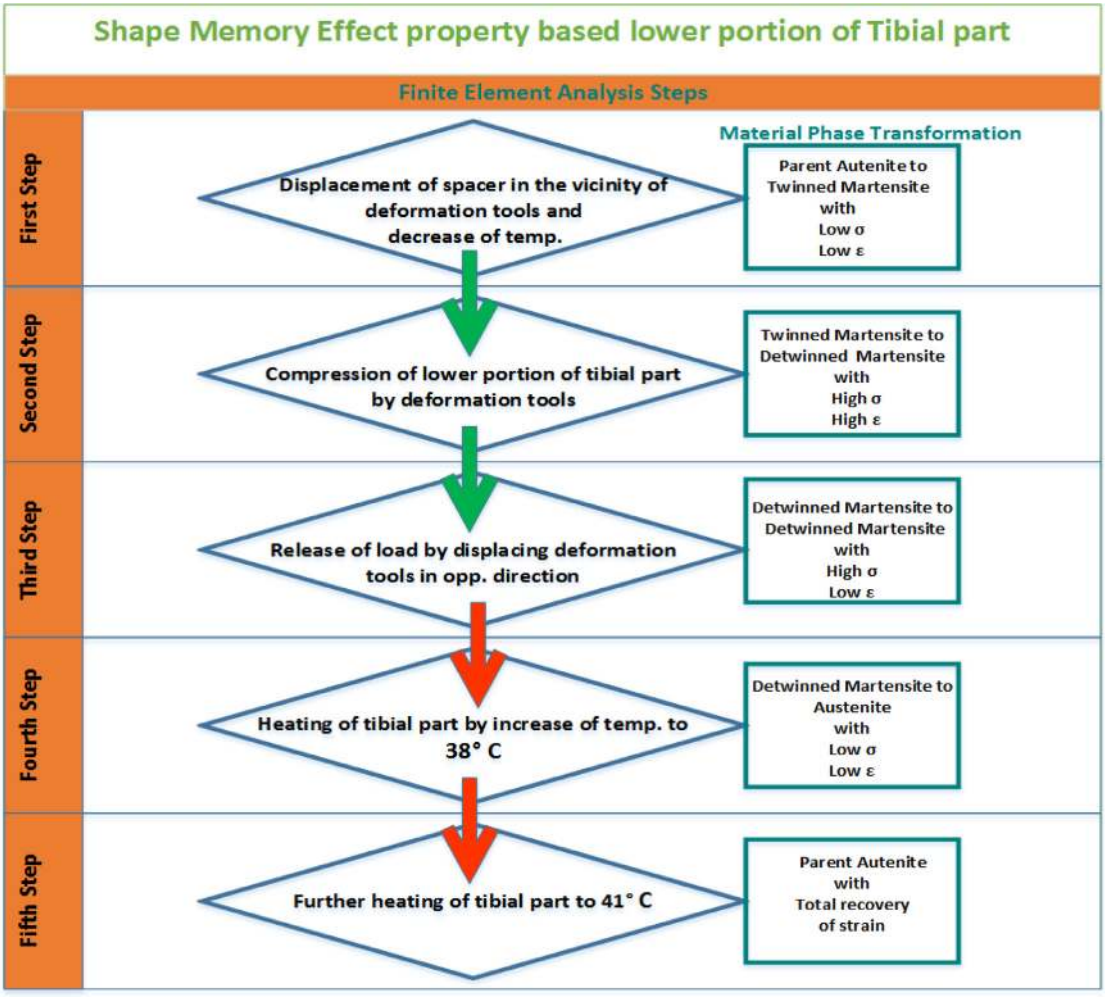


**Figure 5.** Flow-chart of the FEA for the SME property based on the lower portion of the tibial component.

body temperature of 38 °C); therefore, a thermal condition was applied in the proposed model. Because of the applied heat, the total deformation was recovered by the expansion of the lower portion. Thus, the expansion of the lower portion of the tibial component pushed the tibia bone across its circumference. This showed that the SME property of the NiTi SMA stabilised the tibial component on asymmetrical loading at different flexion angles. The complete simulation was carried out in five steps, as shown in the flow-chart in Figure 5. Each step consisted of a minimum of 60 and a maximum of 2500 sub-steps, as explained below. Each step was performed iteratively in sub-steps to avoid simulation convergence.

1. Step-1: in this step, the spacer was displaced in the negative *Y* axis with a displacement of 48 mm to be near the deformation tools. The temperature also decreased from 25 °C to 22 °C to transform the material from austenite to twinned martensite with low-stress and low-strain values.
2. Step-2: in this step, the deformation tools were used to apply load by compressing the lower portion of the tibial component by 2 mm at a temperature of 22 °C. This transformed the material from twinned martensite to detwinned martensite with high-stress and high-strain values.
3. Step-3: in this step, the load from the deformation tools was removed by displacing them in the opposite direction by 40 mm at a temperature of 22 °C. Thus, the lower portion of the tibial component was permanently deformed into the detwinned martensite phase with low-stress and high-strain values.
4. Step-4: in this step, the temperature of the tibial component increased to body temperature, i.e., 38 °C, which transformed the material from detwinned martensite to the austenite phase with low-stress and low-strain values.
5. Step-5: in this step, the temperature increased to 41 °C, and the material was transformed to the parent austenite phase with total recovery of the strain.

### 3.1.3. Fatigue analysis

Fatigue of the NiTi SMA can be classified into two types: functional fatigue and structural fatigue. Functional fatigue of the SMA is not accepted widely by the fatigue research community, according to Mahtabi et al. [45] despite some studies in the literature by Miyazaki et al. [46] and Eggeler et al. [47]. Unlike other materials, the SMA alloy also experiences structural fatigue owing to cyclic loading. The stress and strain life-based methodologies can predict the lifetime of the material through the fatigue behaviour. Although, to study the long-term functionality of the strength of the proposed SMA-based NiTi alloy for the tibial component, the strain life-based fatigue analysis was adopted using the FEA in ANSYS. The strain life fatigue was adopted because of the findings from the studies by Browell and Hancq [48] and Bannantine et al. [49], which are listed below.

1. The strain can be directly measured and can characterise the low-cycle and high-cycle fatigues.

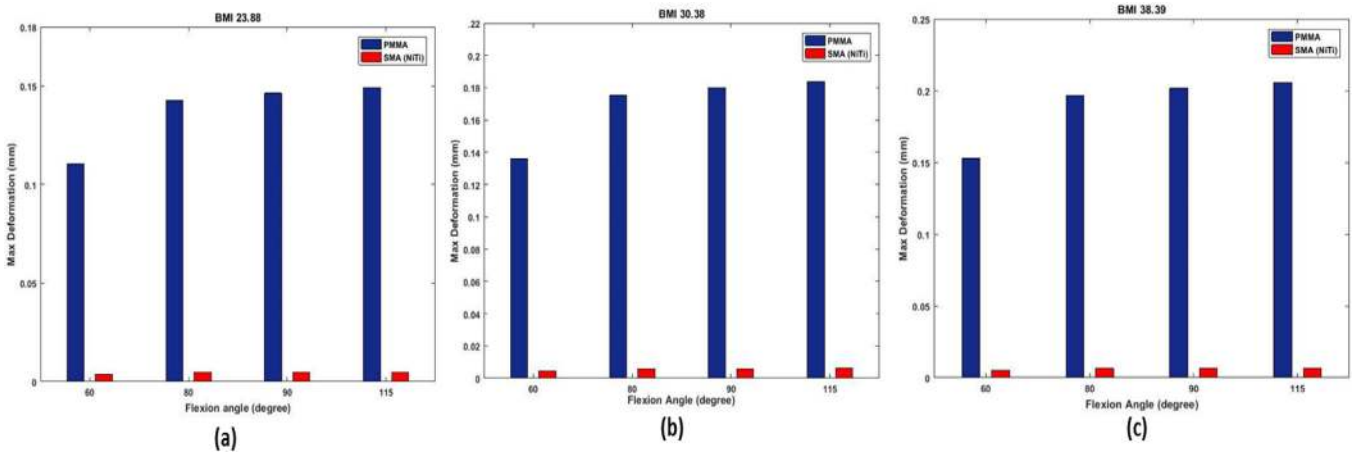


**Figure 6.** (a) Comparison plot for the max deformation at different flexion angles for a BMI of 23.88. Image (b) shows a comparison plot for the max deformation at different flexion angles for a BMI of 30.38. Image (c) shows a comparison plot for the max deformation at different flexion angles for a BMI of 38.39.

**Table 3**
Representative parameter for the fatigue behaviour of NiTi.

| Strain life parameter | Value |
|---|---|
| Cyclic strain hardening exponent | 0.1 |
| Cyclic strength coefficient | 733 MPa |
| Fatigue strength exponent | −0.06 |
| Fatigue strength coefficient | 705 MPa |
| Fatigue ductility exponent | −0.6 |
| Fatigue ductility coefficient | 0.68 |

2. The Strain life is based on crack initiation, whereas stress life is based on the total life and does not distinguish between initiation and propagation.

In this study, the fatigue parameters of NiTi listed in Table 3 were used from the study by Cheung et al. [50]. In the FEA, the factors of the fatigue tools, such as the life, safety factor, and fatigue sensitivity, were studied for the PE and SME tibial component, and the infinite fatigue life (also known as the endurance limit) was defined as $10^9$ cycles.

## 4. Results and discussion

### *4.1. PE property-based tibial component*

The upper portion of the 3D CAD model of the tibial component of TKA was tested for the PE property and verified by the simulation results. A comparative study of the maximum deformation and equivalent (von-Mises) stress with the PMMA-based spacer was performed with the same boundary conditions (from Figure 2) for three different people (BMIs of 23.88, 30.38, and 38.39), as shown in Figures 6 and 7. A person with a BMI greater than 25 is prone to knee osteoarthritis [5–9]. In the validation process, the study was restricted to three subjects based on their BMI to evaluate the efficacy of the proposed model for three category of BMI: healthy, overweight and obese. From Figure 5, for all three subjects, the proposed SMA-based spacer achieved 96.66978% less deformation with a standard deviation of 0.0174 than that of the PMMA-based technology for flexion angles of 60°, 80°, 90°, and 115°.

Based on the maximum deformation analysis from Figure 6, the PMMA-based spacer contained 30 times more permanent deformation than that of the SMA-based spacer for the same load and flexion angle. Furthermore, the deformation of the SMA-based spacer was recoverable when the load was released owing to the PE property of the SMA. The simulation results obtained for all three subjects showed that the SMA-based spacer provided less recoverable total deformation under asymmetric loading, whereas the PMMA-based spacer provided a more permanent deformation. This was one of the main causes of dysfunction of the PMMA-based spacer after treatment in TKA.

From Figure 7, the SMA-based spacer absorbed more stress than that of the PMMA-based spacer for the same loading and flexion angle. The PE property of the SMA used for the development of the upper portion of the tibial component absorbed a large amount of stress and produced less recoverable deformation from a heavy load under asymmetrical loading at different flexion angles during different activities of daily life, such as walking on a level ground, walking on inclined or declined surfaces, and walking downstairs or upstairs.

For the proposed model, the maximum operating temperature was approximately 40 °C, and as per Oppenheimer et al. [54], for equiatomic NiTi, the creep range corresponding to the homologous temperature was 12.5 to 22.5 times greater than the operating temperature of the proposed model (corresponding to the homologous temperature 0.61–0.80, using the melting point of 1310 °C for equiatomic NiTi from the study by Dieter [55]). Thus, from the stress analysis, the PE property of NiTi did not undergo creep-permanent deformation.

The upper portion of the tibial component was subjected to continuously varying cyclic loading owing to its usage application. The fatigue analysis of the material was used to estimate the lifetime of the product. Therefore, the fatigue analysis of the proposed NiTi SMA was required and has been a topic of an interest for material scientists and researchers for two decades [45]. The experimental results for the fatigue of NiTi by Miyazaki et al. [51], Pelton et al. [52], and Pelton et al. [56] using the strain life fatigue analysis showed $10^7$ life cycles for the strain percentage of 0.4. In Azaouzi et al. [53], the fatigue life of NiTi was also dependent on the size and shape of the model.

Therefore, to predict the fatigue life of the proposed PE-based tibial component, the FEA analysis was performed through the fatigue tool in ANSYS Workbench for the life, safety factor, and fatigue sensitivity. From the FEA of the fatigue life, the NiTi-based upper portion of the tibial component showed a minimum fatigue life of $10^9$ cycles, a minimum safety factor of 15, and a fatigue sensitivity of $10^9$ available life cycles for different loading histories with lower and upper variations of 50% and 150% of the applied load, as shown in Figure 8(a).

Thus, the PE property of the SMA-based upper portion of the tibial component would eliminate the drawbacks of spacer fracture and knee subluxation.

Please cite this article as: A. Gautam et al., Shape-memory-alloy-based smart knee spacer for total knee arthroplasty: 3D CAD modelling and a computational study, Medical Engineering and Physics (2018), https://doi.org/10.1016/j.medengphy.2018.03.001

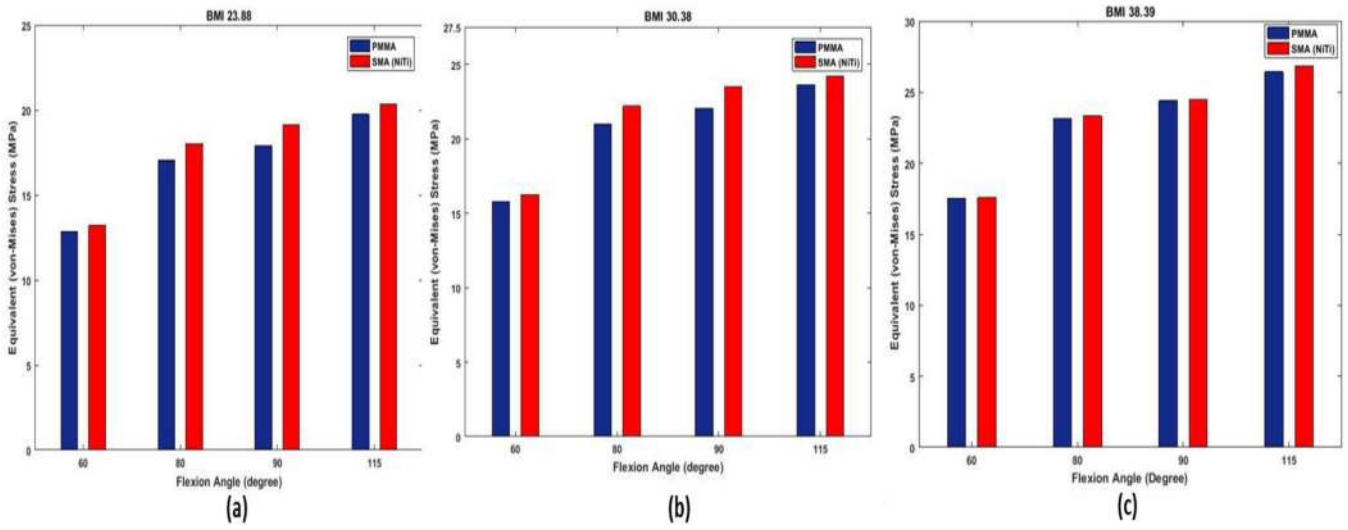


**Figure 7.** (a) Comparison plot for the equivalent (von Mises) stress at different flexion angles for a BMI of 23.88. Image (b) shows a comparison plot for the equivalent (von Mises) stress at different flexion angles for a BMI of 30.38. Image (c) shows a comparison plot for the equivalent (von Mises) stress at different flexion angles for a BMI of 38.39.

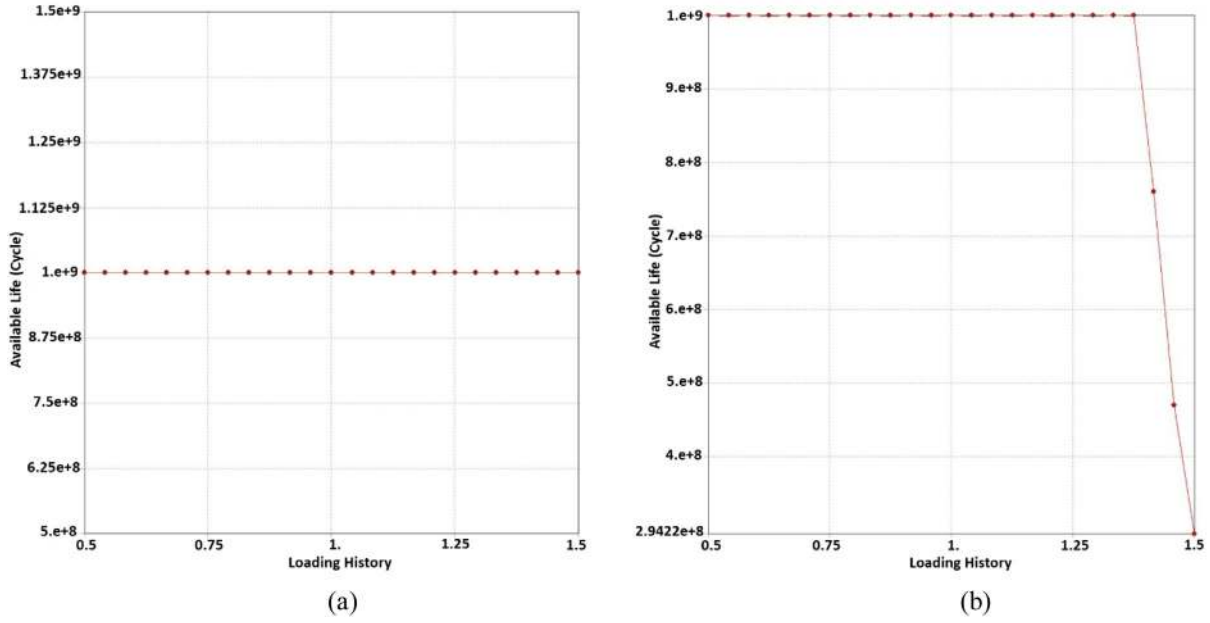


**Figure 8.** (a) Fatigue sensitivity plot for the PE property-based tibial component. Image (b) shows the fatigue sensitivity plot for the SME property-based tibial component.

*4.2.2. SME property-based tibial component*

The 3D CAD model of the lower portion of the tibial component of TKA was tested for the SME property and verified by the simulation results shown in Figure 9. From Figure 9, after the second step of the simulation, the deformation tool compressed the hollow lower portion of the tibial component by 2 mm, and total deformation was recovered in the fourth and fifth steps of the simulation, when the temperature of the hollow lower portion of the tibial component increased to body temperature (38 °C). This produced a maximum of 1139.2 MPa of the total equivalent stress, which allowed the lower portion of the tibial component (which was inserted into the tibia bone) to push and apply pressure to the tibia bone along its circumference. Thus, the SME property fixed the spacer in its position at different asymmetrical loading, unlike the PMMA spacer counterpart.

The present application of the SME property-based tibial component was intended for one-time actuation. Although, fatigue owing to external loading might occur; therefore, the FEA of the fatigue life was performed through the fatigue tool in ANSYS Workbench for the life, safety factor, and fatigue sensitivity. From the FEA of the fatigue life, the NiTi-based lower portion of the tibial component showed a minimum fatigue life of $10^9$ cycles, a minimum safety factor of approximately 1.4, as shown in Figure 9(c), and a fatigue sensitivity of $10^9$ available life cycles for the loading history from 50% to 137.5% of the applied load. Then, there was a linear decrement to $2.9422 \times 10^8$ available life cycles till 150% of the applied load, as shown in Figure 8(b).

The FEA results of the fatigue were compared with the experimental findings in the studies by Pelton et al. [52,56] for the strain amplitude verses the fatigue data (strain-life). This comparison was performed for the worst load condition (a BMI of 38.39 and a flexion angle of 115°) of the PE property-based upper portion. The comparison is listed in Table 4. The results were similar to the experimental findings in the literature.

Please cite this article as: A. Gautam et al., Shape-memory-alloy-based smart knee spacer for total knee arthroplasty: 3D CAD modelling and a computational study, Medical Engineering and Physics (2018), https://doi.org/10.1016/j.medengphy.2018.03.001

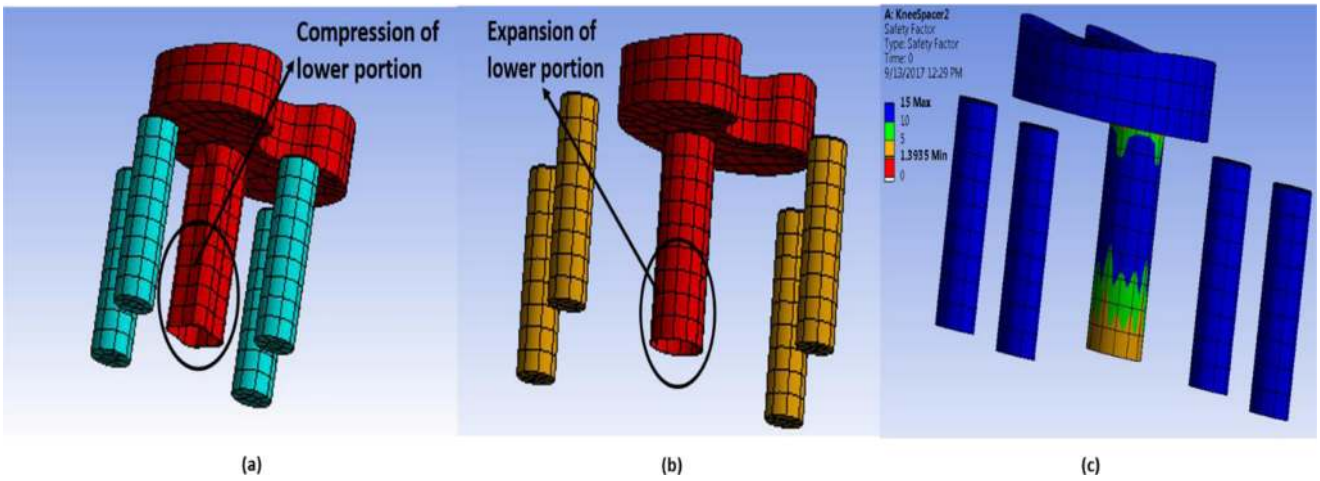


**Figure 9.** Simulation of the SME of the lower portion of the tibial component. Image (a) shows the deformed lower portion from the tools after the second step of the simulation. Image (b) shows the shape recovery of the deformed lower portion of the tibial component after the fourth and fifth step of the simulation. Image (c) shows the contour plot for the safety factor analysis of the lower portion.

**Table 4**
Comparison of the fatigue results by the FEA with the experimental findings in the literature.

| Fatigue studies | Strain amplitude | Number of cycle |
|---|---|---|
| Pelton et al. [52,56] | 0.004 | Minimum $10^7$ |
| Our study (PE property-based upper portion) | 0.00044921 | $10^9$ |

Thus, the FEA results of the PE, SME, and fatigue verified that the proposed SMA-based spacer would overcome the drawbacks of the PMMA-based spacer, which included spacer fracture, loosening, dislocation, tilting or translation, and knee subluxation of the spacers, for asymmetric loading at different flexion angles

## 5. Conclusion

A longer-lasting, more consistent, and higher wear and tear resistant tibial component for TKA was designed using the PE and SME properties of the NiTi SMA. The maximum deformation analysis showed that the PMMA-based spacer contained 30 times more permanent deformation than that of the proposed SMA-based spacer for the same load and flexion angle. In addition, deformation of the SMA spacer was recoverable once the load was released because of its PE property. The simulation results of the SME property for the lower portion of the tibial component showed the SME property fixed the spacer in its position. Subsequently, the results based on CAD modelling followed by the FEA verified this result.

The results presented by the computational studies on the SMA indicated a high potential for designing, development, and optimisation of medical devices based on the NiTi SMA. Recent studies by Gautam et al. [57,58] showed enhanced controllability in shape recovery of the SMA alloy by embedding nano-ferromagnetic particles in the NiTi SMA. This could have numerous real life applications for this new class material. The shape recovery of the SMA for the SME property could be controlled by the antagonistic effect of the magnetic field and temperature. For example, in the treatment of scoliosis using the SMA spinal intervertebral spacer and SMA scoliosis correction device, the abrupt recovery of the shape of the SMA results in failure in surgery and causes pain to the patient. These could be avoided by using the controlled antagonistic effect of the magnetic field and temperature. Therefore, enhancing the controllability in shape recovery during the actuation for the SME effect of the SMA in the magnetic field and temperature change could be a reasonable solution and is achievable by nano-ferromagnetic particle doped NiTi SMA. Thus, this new class of porous NiTi doped nano-ferromagnetic SMA could replace the traditional SMA in the research for biomedical devices based on the NiTi SMA from our future research.

## Acknowledgements

The Arvind Gautam research was supported by Visvesvaraya PhD Scheme for Electronics and IT by the Ministry of Electronics and Information Technology (MeitY), India, and Indian Institute of Technology Hyderabad, Hyderabad. Amit Acharyya and Swati Ghosh Acharyya acknowledge the Visvesvaraya PhD scheme by MeitY, India and University of Hyderabad (UOH) Hyderabad, India for this research.

## Conflict of interest

No conflict of interest is declared.

## Funding

This research was funded by the Visvesvaraya PhD Scheme for Electronics and IT by the Ministry of Electronics and Information Technology (MeitY), India, and the Indian Institute of Technology Hyderabad, Hyderabad, India.

## Ethical Approval

Ethical approval is not applicable.

## Reference

[1] Felson DT, Lawrence RC, Dieppe PA, Hirsch R, Helmick CG, Jordan JM, Sowers M. Osteoarthritis: new insights. Part 1: the disease and its risk factors. Ann Intern Med 2000;133(8):635–46.
[2] Peat G, McCarney R, Croft P. Knee pain and osteoarthritis in older adults: a review of community burden and current use of primary health care. Ann Rheum Dis 2001;60(2):91–7.
[3] Cooper C, Snow S, McAlindon TE, Kellingray S, Stuart B, Coggon D, Dieppe PA. Risk factors for the incidence and progression of radiographic knee osteoarthritis. Arthritis Rheum 2000;43(5):995–1000.
[4] Lawrence RC, Helmick CG, Arnett FC, Deyo RA, Felson DT, Giannini EH, Liang MH. Estimates of the prevalence of arthritis and selected musculoskeletal disorders in the United States. Arthritis Rheum 1998;41(5):778–99.
[5] Blagojevic M, Jinks C, Jeffery A, Jordan. Risk factors for onset of osteoarthritis of the knee in older adults: a systematic review and meta-analysis. Osteoarthr Cartil 2010;18(1):24–33.

[6] Sowers MR, Karvonen-Gutierrez CA. The evolving role of obesity in knee osteoarthritis. Curr Opin Rheum 2010;22(5):533.
[7] Coggon D, Reading I, Croft P, McLaren M, Barrett D, Cooper C. Knee osteoarthritis and obesity. Int J Obes 2001;25(5):622.
[8] Jadelis K, Miller ME, Ettinger WH, Messier SP. Strength, balance, and the modifying effects of obesity and knee pain: results from the Observational Arthritis Study in Seniors (OASIS). J Am Geriatr Soc 2001;49(7):884–91.
[9] Powell A, Teichtahl AJ, Wluka AE, Cicuttini FM. Obesity: a preventable risk factor for large joint osteoarthritis which may act through biomechanical factors. Br J Sports Med 2005;39(1):4–5.
[10] Brunnekreef J, Hannink G, Malefijt Mde W. Recovery of knee mobility after a static or mobile spacer in total knee infection. Acta Orthop Belg 2013;79(1):83–9.
[11] Cui Q, Mihalko WM, Shields JS, Ries M, Saleh KJ. Antibiotic-impregnated cement spacers for the treatment of infection associated with total hip or knee arthroplasty. J Bone Joint Surg 2007;89(4):871–82.
[12] Masouros SD, Bull AMJ, Amis AA. (i) Biomechanics of the knee joint. Orthop Trauma 2010;24(2):84–91.
[13] Kuster MS, Wood GA, Stachowiak GW, Gächter A. Joint load considerations in total knee replacement. Bone Joint J 1997;79(1):109–13.
[14] D'Lima DD, Fregly BJ, Patil S, Steklov N, Colwell CW Jr. Knee joint forces: prediction, measurement, and significance. Proc Inst Mech Eng Part H J Eng Med 2012;226(2):95–102.
[15] Kohl S, Evangelopoulos DS, Kohlhof H, Krueger A, Hartel M, Roeder C, Eggli S. An intraoperatively moulded PMMA prostheses like spacer for two-stage revision of infected total knee arthroplasty. Knee 2011;18(6):464–9.
[16] Macmull S, Bartlett W, Miles J, Blunn GW, Pollock RC, Carrington RWJ, Briggs TWR. Custom-made hinged spacers in revision knee surgery for patients with infection, bone loss and instability. Knee 2010;17(6):403–6.
[17] Nickinson RSJ, Board TN, Gambhir AK, Porter ML, Kay PR. Two stage revision knee arthroplasty for infection with massive bone loss: a technique to achieve spacer stability. Knee 2012;19(1):24–7.
[18] Pang H-N, Seah RB, MacDonald SJ. Treatment of infected nonunion total knee arthroplasty periprosthetic fracture using a stemmed articulating spacer. Knee 2015;22(5):440–2.
[19] Shen H, Zhang X, Jiang Y, Wang Q, Chen Y, Wang Q, Shao J. Intraoperatively-made cement-on-cement antibiotic-loaded articulating spacer for infected total knee arthroplasty. Knee 2010;17(6):407–11.
[20] Vaughan N, Dubey VN, Wainwright TW, Middleton RG. A review of virtual reality based training simulators for orthopaedic surgery. Med Eng Phys 2016;38(2):59–71.
[21] Navarro M, Michiardi A, Castano O, Planell JA. Biomaterials in orthopaedics. J R Soc Interface 2008;5(27):1137–58.
[22] Revell PA. The combined role of wear particles, macrophages and lymphocytes in the loosening of total joint prostheses. J R Soc Interface 2008;5(28):1263–78.
[23] Struelens B, Claes S, Bellemans J. Spacerrelated problems in two-stage revision knee arthroplasty. Acta Orthop Belg 2013;79(4):422–6.
[24] Dai XF, Liu GD, Liu ZH, Wu GH, Chen JL, Meng FB, Wang WG. Superelasticity of CoNiGa: Fe single crystals. Appl Phys Lett 2005;87(11):112504.
[25] Petrini L, Migliavacca F, Massarotti P, Schievano S, Dubini G, Auricchio F. Computational studies of shape memory alloy behavior in biomedical applications. J Biomech Eng 2005;127(4):716–25.
[26] Tabesh M, Goel V, Elahinia MH. Shape memory alloy expandable pedicle screw to enhance fixation in osteoporotic bone: primary design and finite element simulation. J Med Devices 2012;6(3):034501.
[27] Jani JM, Leary M, Subic A, Gibson MA. A review of shape memory alloy research, applications and opportunities. Mater Des 2014;56:1078–113 (1980-2015).
[28] Funakubo H. Shape memory alloys. New York: Gordon and Breach Science Publishers; 1987. p. 275.
[29] Suzuki Y, Otsuka K, Wayman CM. Shape memory materials. Cambridge University Press; 1998. p. 137–8.
[30] Ingrassia T, Nalbone L, Nigrelli V, Tumino D, Ricotta V. Finite element analysis of two total knee joint prostheses. Int J Interact Des Manuf (IJIDeM) 2013;7(2):91–101.
[31] Bahraminasab M, Sahari BB, Hassan MR, Arumugam M, Shamsborhan M. Finite element analysis of the effect of shape memory alloy on the stress distribution and contact pressure in total knee replacement. Trends Biomater Artif Organs 2011;25(3):95–100.
[32] Godest AC, Beaugonin M, Haug E, Taylor M, Gregson PJ. Simulation of a knee joint replacement during a gait cycle using explicit finite element analysis. J Biomech 2002;35(2):267–75.
[33] Chow JW. Knee joint forces during isokinetic knee extensions: a case study. Clin Biomech 1999;14:329338.
[34] Kuster M, Sakurai S, Wood GA. Kinematic and kinetic comparison of downhill and level walking. Clin Biomech 1995;10(2):7984.
[35] Gautam A, Bhargavi Rani A, Callejas MA, Acharyya SG, Acharyya A, Biswas D, Bhandari V, Sharma P, Naik GR. Shape memory alloy smart knee spacer to enhance knee functionality: model design and finite element analysis. In: Proceedings of the thirty-eighth IEEE annual international conference of the engineering in medicine and biology society (EMBC). IEEE; 2016. p. 6046–9.
[36] Otsuka K, Wayman CM. Mechanism of shape memory effect and superelasticity. Shape Mem Mater 1998:27–49.
[37] Buehler WJ, Gilfrich JV, Wiley RC. Effect of lowtemperature phase changes on the mechanical properties of alloys near composition TiNi. J Appl Phys 1963;34(5):1475–7.
[38] Otsuka K, Wayman CM. Shape memory materials. Cambridge University Press; 1999.
[39] Duerig TW, Pelton AR. Ti-Ni shape memory alloys. Materials properties handbook: titanium alloys. American Society for Metals; 1994. p. 1035–48.
[40] Collins JJ. The redundant nature of locomotor optimization laws. J Biomech 1995;28:251–67.
[41] Morrison JB. Function of the knee joint in various activities. Biomed Eng 1969;4:573–80.
[42] Andriacchi PT, Andersson GBJ, Fermier RW, Stern D, Galante JO. A study of lower-limb mechanics during stair-climbing. J Bone Joint Surg 1980;62-A:749–57.
[43] Morrison JB. The mechanics of the knee joint in relation to normal walking. J Biomech 1970;3:51–61.
[44] Harrington IJ. A bioengineering analysis of force actions at the knee in normal and pathological gait. Biomed Eng 1976;11:167–72.
[45] Mahtabi MJ, Shamsaei N, Mitchell MR. Fatigue of Nitinol: the state-of-the-art and ongoing challenges. J Mech Behav Biomed Mater 2015;50:228–54.
[46] Miyazaki S, Imai T, Igo Y, Otsuka K. Effect of cyclic deformation on the pseudoelasticity characteristics of Ti-Ni alloys. Metall Trans A 1986;17(1):115–20.
[47] Eggeler G, Hornbogen E, Yawny A, Heckmann A, Wagner M. Structural and functional fatigue of NiTi shape memory alloys. Mater Sci Eng A 2004;378(1–2):24–33.
[48] Browell R, Hancq A. "Calculating and displaying fatigue results." ANSYS® Online White Papers, March 29 (2006).
[49] Bannantine JA, Comer JJ, Handrock JL. Fundamentals of metal fatigue analysis. Upper saddle river: Prentice Hall; 1989. p. 38.
[50] Cheung GSP, Zhang EW, Zheng YF. A numerical method for predicting the bending fatigue life of NiTi and stainless steel root canal instruments. Int Endod J 2011;44(4):357–61.
[51] Miyazaki S, Mizukoshi K, Ueki T, Sakuma T, Liu Y. Fatigue life of Ti–50 at.% Ni and Ti–40Ni–10Cu (at.%) shape memory alloy wires. Mater Sci Eng A 1999;273:658–63.
[52] Pelton AR, Fino-Decker J, Vien L, Bonsignore C, Saffari P, Launey M, Mitchell MR. Rotary-bending fatigue characteristics of medical-grade Nitinol wire. J Mech Behav Biomed Mater 2013;27:19–32.
[53] Azaouzi M, Makradi A, Belouettar S. Deployment of a self-expanding stent inside an artery: a finite element analysis. Mater Des 2012;41:410–20.
[54] Oppenheimer SM, Yung AR, Dunand DC. Power-law creep in near-equiatomic nickel–titanium alloys. Scr Mater 2007;57(5):377–80.
[55] Dieter GE. Mechanical metallurgy, SI metric edition. New York: McGraw-Hill Book Company; 1988.
[56] Pelton AR, Schroeder V, Mitchell MR, Gong XY, Barney M, Robertson SW. Fatigue and durability of Nitinol stents. J Mech Behav Biomed Mater 2008;1(2):153–64.
[57] Gautam A, Balouria A, Andem D, Mounika K, Rani AB, Acharyya A, Acharyya SG. Thermo-magnetic control system for nano-ferromagnetic particle doped shape memory alloy for orthopedic devices and rehabilitation techniques. J Low Power Electron 2017;13(4):678–86.
[58] Gautam A, Balouria A, Acharyya A, Acharyya SG, Panwar M, Naik GR. Shape memory effect of nano-ferromagnetic particle doped NiTi for orthopedic devices and rehabilitation techniques. In: Proceedings of the thirty-ninth annual international conference on engineering in medicine and biology society (EMBC). IEEE; 2017. p. 950–3.

Please cite this article as: A. Gautam et al., Shape-memory-alloy-based smart knee spacer for total knee arthroplasty: 3D CAD modelling and a computational study, Medical Engineering and Physics (2018), https://doi.org/10.1016/j.medengphy.2018.03.001